Arch. Metall. Mater. **67** (2022), 3, 1125-1136

DOI: https://doi.org/10.24425/amm.2022.139712

A. GARBACZ-KLEMPKA[1*], M. PIĘKOŚ[1], M. PEREK-NOWAK[2], J. KOZANA[1], P. ŻAK[1], A. FIJOŁEK[1], P. SILSKA[3], M. STRÓŻYK[3]

RECONSTRUCTION OF THE LATE BRONZE AGE FOUNDRY PROCESS IN GREATER POLAND: ANALYZES AND SIMULATIONS. CASE STUDY OF HOARD FROM PRZYBYSŁAW

One of the most interesting categories of artifacts for archaeometallurgical research includes deposits of bronze items, so-called "metallurgists hoards". They contain, aside of final products, many fragments of raw material and, moreover, metallurgical tools. An important source for the studies on the history of metallurgical technology is hoard from Przybysław, Greater Poland district.

Thus, the aim of the work is the identification and interpretation of bronze-working practices and strategies adopted by prehistoric communities of the Late Bronze Age and the Early Iron Age (ca. 600 BC). The examined objects are characterized in terms of their design, structure, and chemical composition. The methods chosen for the studies of artifacts include: metallographic macro- and microscopic observations using optical microscopy (OM) and scanning electron microscopy (SEM), the analysis of chemical composition with the methods of energy dispersive X-ray spectroscopy (EDS), and X-ray fluorescence (ED-XRF).

The thermodynamic analysis of the alloys was performed on the basis of the CALPHAD method. The experimental melts allowed to verify the theoretical considerations and to determine the characteristic temperatures of changes.

The old casting technology can be analyzed basing on computer modeling and computer simulation methods. Simulations in the MAGMASOFT® software are a good example to illustrate how to fill a mould cavity with a molten bronze for a hoop ornament. It is also an appropriate tool to determine temperature distribution in a mould. The simulations also show the possible disadvantages with this old technology.

Keywords: Archaeometallurgy; Copper Alloys; Casting; CALPHAD; Computer modeling; Late Bronze Age

1. Introduction

Scientific analytical methods as well as computer-aided methods for technological processes have considerable effect in understanding and visualization of casting technology. Studies on the ancient metallurgical/casting processes include many aspects: starting with the analysis of the ores, metallurgical semi-products, slag, and final products, to tools, crucibles, shank ladles and casting moulds [1-7].

In the development of casting techniques, the technology of precision casting by the melt-pattern method (lost wax method) was of the greatest importance. Earthen moulds were used to cast both small ornaments, complicated in shape and decoration, and massive simple bracelets and necklaces [3,14-16]. The beeswax models were glued with clay, the moulds were dried and fired, ensuring the mould withstand high temperature and durability in contact with liquid metal. During the heat treatment of the mould, the wax was melted from the inside of the mould. The mould prepared in this way was poured with liquid melt through a gating system with a gating tank. After the alloy crystallization process was completed, a cast with a prepared shape was obtained. This method ensured a significant smoothness of the casting surface, important for aesthetic reasons, and the accuracy of model reproduction [15,17].

The properly conducted production process of castings with appropriate operational and aesthetic properties required special knowledge and experience. The level of evaluation of this experience is possible on the basis of the preserved evidence in the form of moulds and casts with the use of modern research methods and computer-aided processes [18-20].

[1] AGH UNIVERSITY OF SCIENCE AND TECHNOLOGY, FACULTY OF FOUNDRY ENGINEERING, HISTORICAL LAYERS RESEARCH CENTRE, KRAKÓW, POLAND
[2] AGH UNIVERSITY OF SCIENCE AND TECHNOLOGY, FACULTY OF NON FERROUS METALS, HISTORICAL LAYERS RESEARCH CENTRE, KRAKÓW, POLAND
[3] ARCHAEOLOGICAL MUSEUM IN POZNAŃ, POZNAŃ, POLAND

* Corresponding author: agarbacz@agh.edu.pl

2. Materials and methods

The presented hoard was discovered in Przybysław (Fig. 1), Greater Poland, Jarocin district on the necropolis area associated with Lusatian Culture communities [21-22]. Based on typochronological analysis the discovered finds are dated to the period HaD (Hallstatt D), i.e. around 600 BC [23-24]. Due to the presence of metal raw material and scrap in the composition of the hoard, it is associated with metallurgical activity. The mentioned case also belongs to a rare group of bimetallic raw material hoards from area of Poland [25-26].

Fig. 1. Hoard found in Przybysław including three lumps of bronze raw material, two lumps of iron raw material, six fragments of four necklaces and a socketed axe

The aim of the research was to analyze the process of casting one of the necklaces in the form of a single-use clay, the so-called destroyed form, on the basis of the obtained experimental and simulation data. An additional task was to recreate the virtual geometry of the necklace casting, and then to produce foundry equipment that would allow the simulation of the entire casting process in the MAGMASOFT® software.

The macro- and microscopic examinations were carried out with the use of the NIKON SMZ 745T stereoscopic microscope with a digital camera and the Nis-Elements image analysis system.

The chemical composition was determined by X-ray fluorescence spectrometry with the use of energy dispersive X-ray fluorescence spectrometer (ED-XRF), Spectro Midex equipped with an X-ray tube with Mo anode and Si SDD semiconductor detector. The microstructure observation and determination of elements present in microareas were performed using Hitachi S-3400N scanning electron microscope (SEM) with an attachment for energy dispersive X-ray spectroscopy (EDS) by Thermo Noran. Thermodynamic study of the Cu-Pb-Sn-Ag-Bi multiphase alloy was carried out using the CALPHAD (CALculation of PHAse Diagrams) method using the Thermo-Calc package with the TCCU copper alloy base: TCS Cu-based Alloys Database and based on the analysis of equilibrium systems [27-33]. With the use of this method, transformations and phase composition of the alloys were predicted. The obtained data was verified on the basis of an experimental model alloy melt. The experiment was carried out by composing the alloy from pure components with the same chemical composition as the starting alloy, melting it and casting successively: to a sand, ceramic and metal mould. The modeling results were verified on the basis of the chemical composition and thermal analysis curves (ATD).

The geometric visualization of the cast necklace was made using computer modeling in the SOLIDWORKS program on an example Figs. 2-3, while the processes of pouring and solidifying the castings were simulated in the MAGMASOFT® software. Laboratory data and thermophysical calculations were used for the simulation.

Fig. 2. Fragments of the necklace from Przybysław

Fig. 3. Reconstruction of the necklace on the basis of preserved fragments, P. Silska

This enabled the visualization and better understanding of foundry processes in the field of mould preparation, casting and solidification of the alloy in the mould. It also allowed us to assess the correctness of the technology in terms of the occurrence of defects in castings.

3. Experimental results

The results of analytical research were used in modeling and computer simulations. The results of the chemical composition analysis, together with microstructure observations, were used in the thermodynamic simulations using the CALPHAD method.

They were also used in the experiment of casting a model alloy corresponding to the chemical profile of the necklace. The thermal analysis performed during the crystallization of the alloy allowed us to verify the theoretical data obtained as part of the thermodynamic analysis of the alloy prepared in the Thermo-Calc software. The information entered into the MAGMASOFT® software enabled the simulation of pouring and solidification and indicated the probability of defects occurring precisely for this alloy.

Chemical composition and microstructure analysis

The necklace consists of two connected coils tapering towards the top. As shown by macroscopic analysis, it was made using a casting technique using the precision casting by means of lost wax casting technique in a disposable clay mould. The sequence of geometric ornaments was made directly on the wax model (Figs. 4-5).

The chemical composition analysis was performed by ED-XRF. The average results of the measurements of both pieces of the preserved necklace (marked as a and b) are presented in TABLE 1.

TABLE 1

Chemical composition of necklace from Przybysław by ED-XRF (wt%)

Chemical Composition (wt%)									
Fe	Ni	Cu	Zn	As	Ag	Sn	Sb	Pb	Bi
0.03	0.13	89.73	0.13	0.32	0.09	2.37	0.09	6.44	0.59

The analysis shows that the necklace was cast from lead-tin bronze, containing 6.4% Pb and 2.4% tin. In the thermodynamic analysis of the alloy, the following additives are also important, being traces of copper ore origin: 0.6% Bi, 0.3% As, 0.1% Sb, 0.1% Ag and 0.1% Ni and Zn. The microarea composition analysis was performed using a scanning electron microscope and an EDS non-dispersive analysis system. Visible dendritic structure proving the casting of the necklace. Precipitations do not show traces of deformation as a result of plastic processing. Detailed analysis of the chemical composition in micro-areas is presented in the form of a table and a map of the distribution of elements. The exemplary images of the necklace's microstructure show a dendritic structure with numerous precipitates of intermetallic phases (Figs 6-8). Between the dendrites of the solid solution α; there is a small amount of eutectoid and phases containing lead,

Fig. 4. One of the two preserved parts of the necklace Przy_184b-b

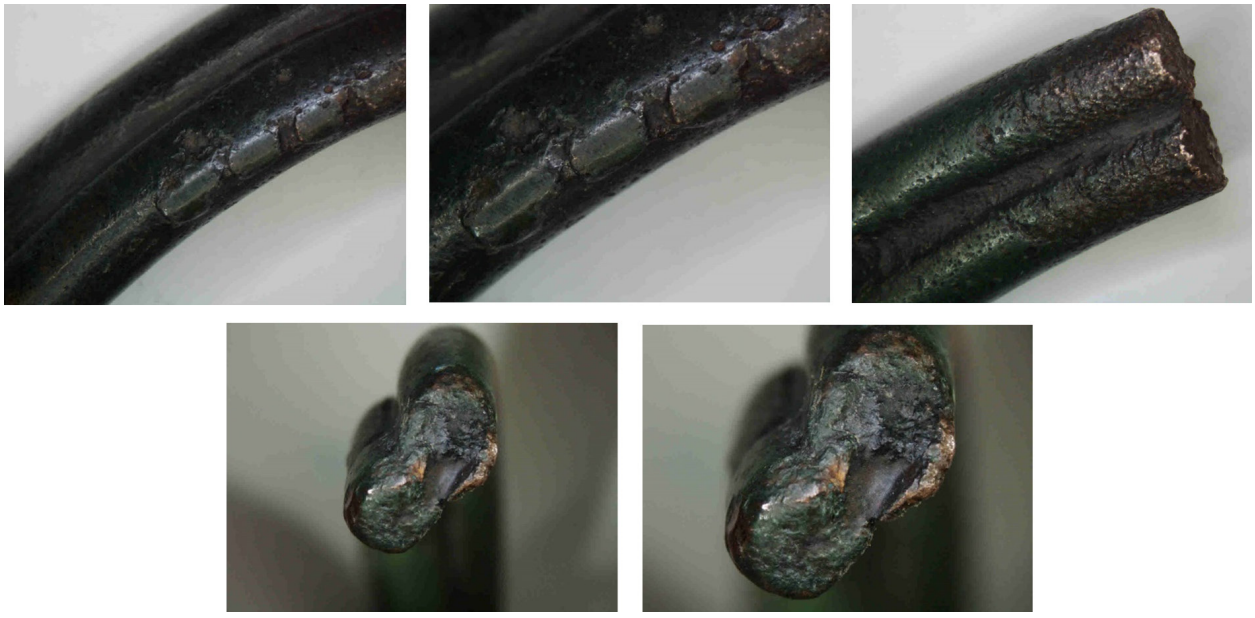

Fig. 5. One of the two preserved parts of the necklace Przy_184b-a

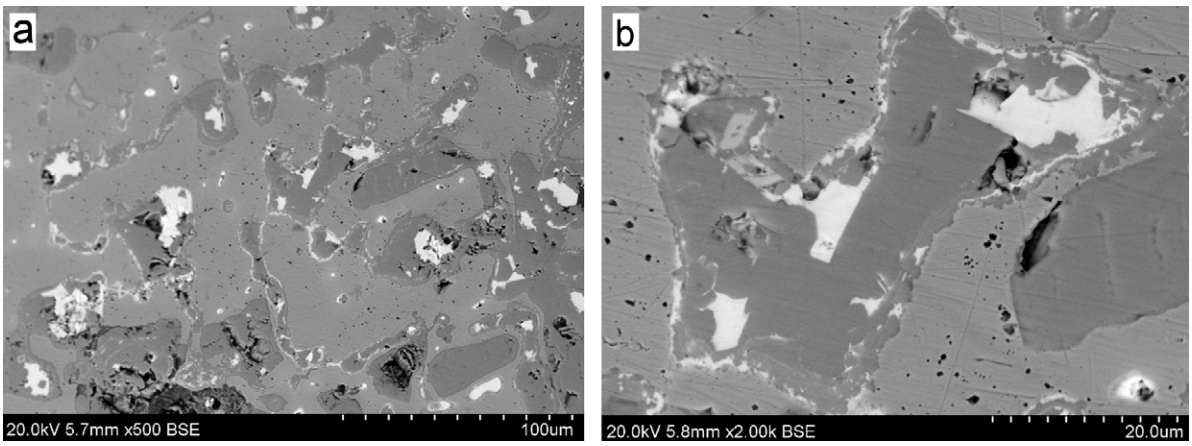

Fig. 6. Microstructure of the necklace from the treasure in the BSE contrast: (a) magnification 500×, (b) 2000×

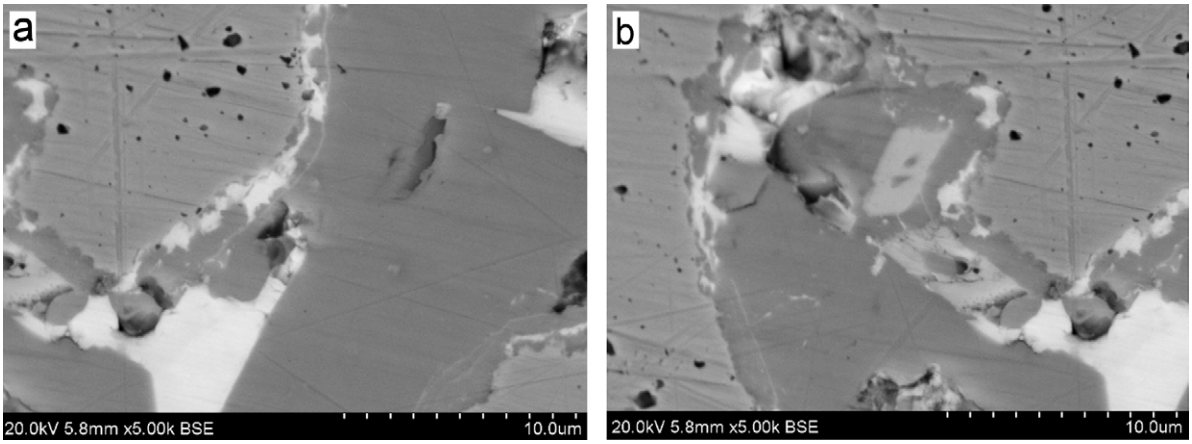

Fig. 7. Microstructure of the necklace from the treasure in the BSE contrast: (a) magnification 500×, (b) 5000×

tin and silver in the presence of copper. Numerous white irregular areas are lead, insoluble in copper, because the system is characterized by the lack of mutual solubility of the components of copper and lead in the solid state and limited solubility in the liquid state (TABLE 2).

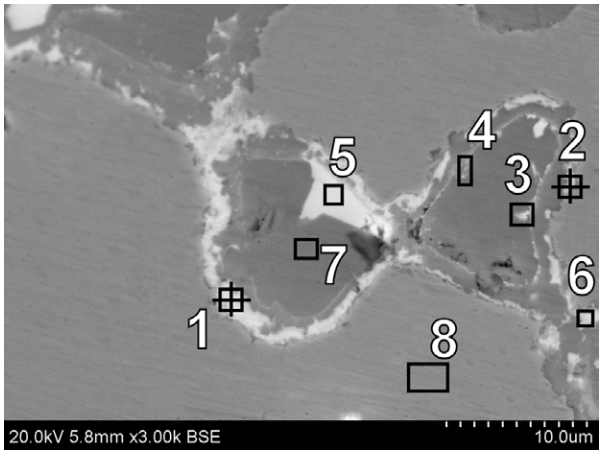

Fig. 8. EDS microanalysis area 3000×

The distribution of elements in the alloy is confirmed by the map of the distribution of elements (Fig. 9-10).

TABLE 2

Chemical composition of necklace from Przybysław in microareas by SEM-EDS (wt%)

	Chemical Composition (wt%)				
Area	**O**	**Cu**	**Ag**	**Sn**	**Pb**
Prz 184b a_pt1		19.01	—	—	80.99
Prz 184b a_pt2		95.85	—	4.15	—
Prz 184b a_pt3		90.09	9.91	—	—
Prz 184b a_pt4		84.03	—	5.21	10.76
Prz 184b a_pt5		10.13	—	—	89.87
Prz 184b a_pt6		87.28	—	2.91	9.81
Prz 184b a_pt7	15.39	84.61	—	—	—
Prz 184b a_pt8		100.00	—	—	—

Experiment and thermodynamic simulation/modeling

In the course of the research, an experiment was carried out consisting in the preparation and casting of a model alloy with a given chemical composition, analogous to a necklace. The castings were made in the shape of a cuboid with a thermocouple placed in its geometric center. Additionally, the alloy was poured into a sand, ceramic and metal mould to indicate differences in

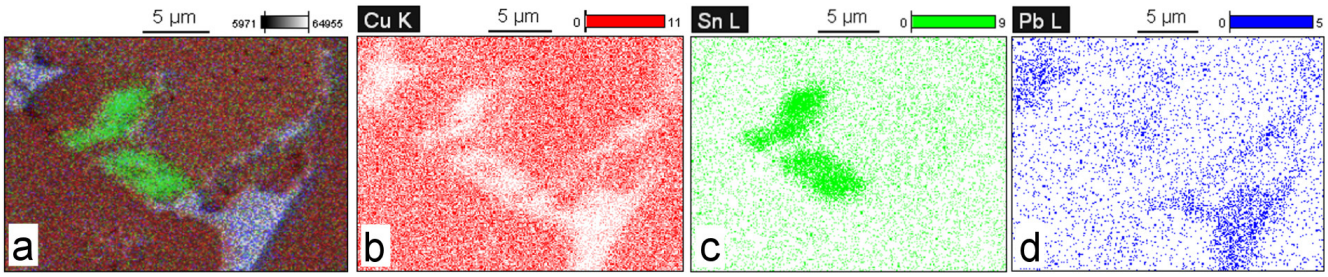

Fig. 9. Map of the distribution of elements for the necklace from the treasure from Przybysław based on SEM-EDS (corresponding to Fig. 7a). The proportion of copper, tin, lead

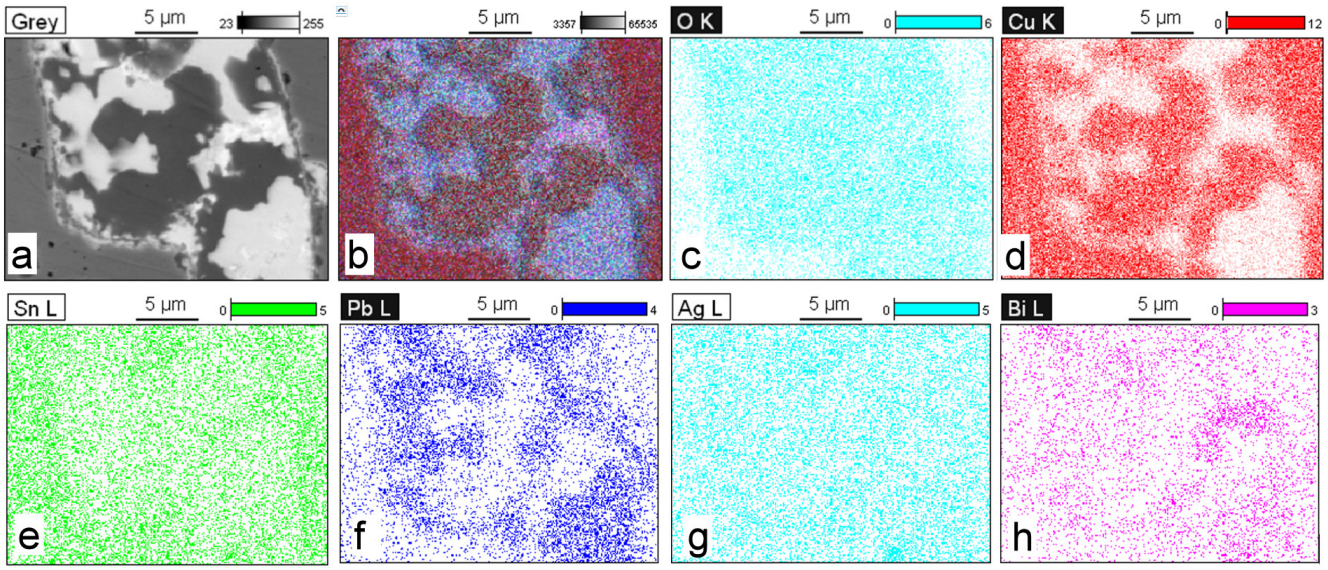

Fig. 10. Map of the distribution of elements for the necklace from the treasure from Przybysław based on SEM-EDS. The proportion of oxygen, copper, tin, lead, silver and bismuth

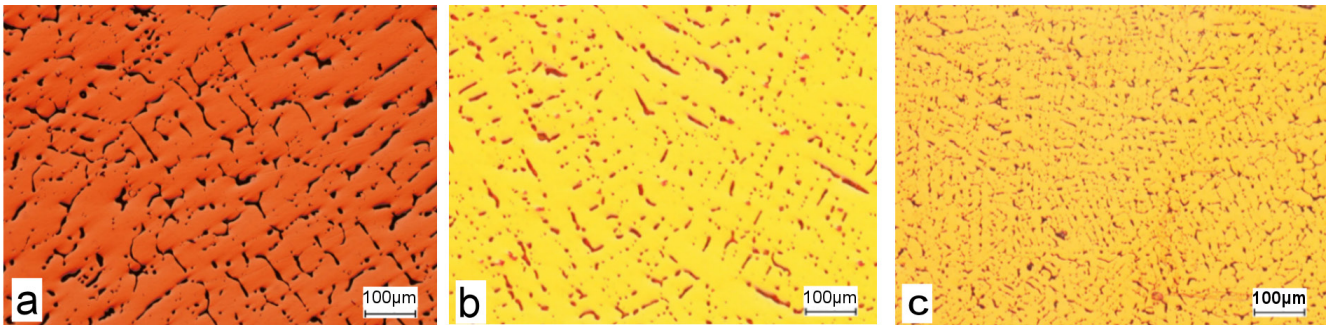

Fig. 11. CuPb6.4Sn2.4 alloy cast into: (a) sand mould, (b) ceramic mould, (c) metal mould

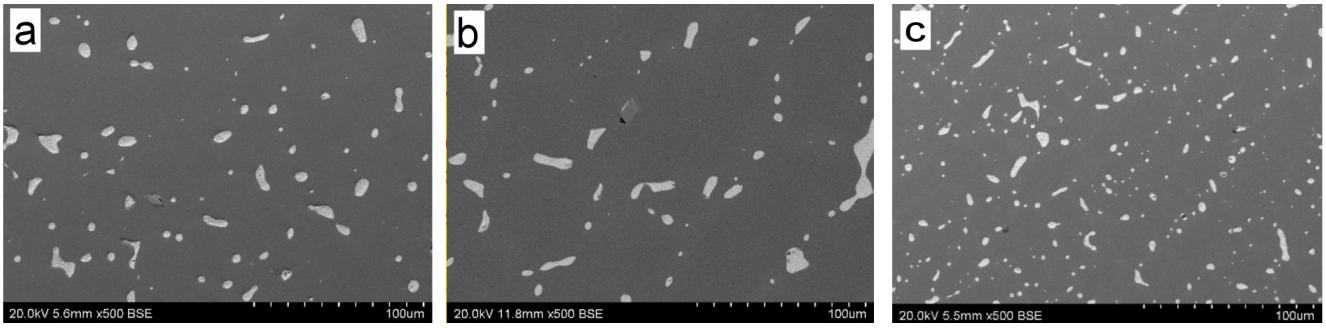

Fig. 12. CuPb6.4Sn2.4 alloy cast into: (a) sand mould, (b) ceramic mould, (c) metal mould

the size of the structural components (Figs. 11-12). The developed cooling curves along with the characteristic temperatures of phase transformations determined on the basis of the ATD thermal derivative analysis are shown in Fig. 13.

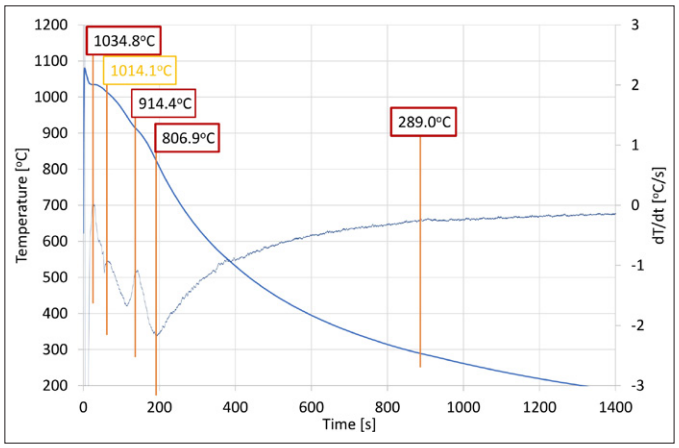

Fig. 13. Values of characteristic temperatures for CuPb6.4Sn2.4Bi0.3 alloy (ATD)

At the same time, the thermodynamic modeling process was carried out with the use of Thermo-Calc software, during which the values of characteristic temperatures and phase compositions that may appear during the crystallization of this alloy were obtained (TABLE 3). Additionally, in order to illustrate fully, the percentage shares of individual phases in the ambient temperature as well as at individual stages of crystallization have been presented.

TABLE 4 presents selected the numerical data of the tests carried out using the TC and ATD methods.

Fig. 14 shows the process of crystallization of the considered alloy through TC modeling as well as the AT crystallization curve recorded during the melts. The characteristic TC modeling temperatures are presented in red, and the experimental thermal analysis AT is presented in blue.

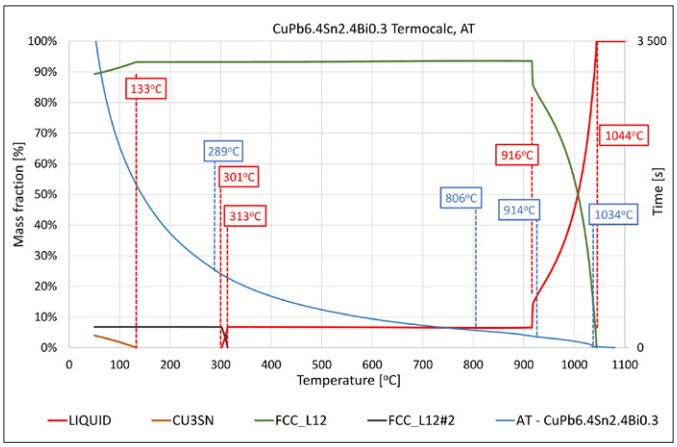

Fig. 14. Results of thermodynamic modeling and thermal analysis of the CuPb6.4Sn2.4 alloy

The theoretical and experimental analysis shows that the crystallization begins at T1 = 1044.4°C (according to Thermo-Calc) and T1 = 1034.8°C (according to ATD), when crystals of α (Cu) solid solution appear, crystallizing in the A1 crystal lattice (FCC_L12). The amount of solid solution is rapidly in-

TABLE 3

Characteristic temperatures and structural components obtained with CALPHAD thermodynamic modeling and thermal analysis

Sample/Phase		Temperature [°C] / Mass Fraction at 50°C [%]						
		T_1	T_2	T_3	T_4	T_5	T_6	T_7
ATD		1034	914	806	—	289	—	—
LIQUID		**1044/90.0**	**916/6.5**	—	—	**301/0**	—	—
Mass percent of LIQUID [%]	Cu	90.8	8.8	—	—	0.04	—	—
	Pb	6.5	86.2	—	—	91.7	—	—
	Sn	2.4	0.4	—	—	0.05	—	—
	Bi	0.3	4.6	—	—	8.2	—	—
FCC_L12		**1044/9.9**	**916/93.5**	—	—	—	**133/93.0**	**50/89.3**
Mass percent of FCC_L12 [%]	Cu	99.2	96.6	—	—	—	97.4	99.0
	Pb	0.3	0.8	—	—	—	0.0002	0
	Sn	0.5	2.6	—	—	—	2.6	1.0
	Bi	0.0004	0.001	—	—	—	0	0
FCC_L12#2		—	—	—	**313/2.9**	—	—	**50/6.8**
Mass percent of FCC_L12#2 [%]	Cu	—	—	—	0.001	—	—	0
	Pb	—	—	—	97.6	—	—	95.6
	Sn	—	—	—	0.004	—	—	0
	Bi	—	—		2.4	—	—	4.4
CU3SN		—	—	—	—	—	**133/0.2**	**50/3.9**
Mass percent of CU3SN [%]	Cu	—	—	—	—	—	61.9	61.7
	Pb	—	—	—	—	—	0	0
	Sn	—	—	—	—	—	38.1	38.3
	Bi	—	—	—	—	—	0	0

TABLE 4

Characteristic temperatures obtained with CALPHAD thermodynamic modeling and thermal analysis

Temperature	Modelling [°C]	Experiment [°C]
Liquidus	1044.4	1034.8
Solidus	301.6	289.0
Change in composition of the primary phase **FCC L12**	916.0	914.4
End of primary phase growth	916.0	806.9*

* – practical end of crystallization based on ATD

creased to reach the value of 93.5% at T2 = 916°C in the case of TC modeling. We observe similar effects on the experimental ATD curve, there are thermal effects, especially the intensely visible T2 = 914°C, which basically completes the crystallization of the alloy at the temperature of T3 = 806.9°C. However, after an in-depth analysis of the derivative curve, a slight spike due to the end of lead crystallization can be observed at T5 = 289°C. The end of crystallization for the assumed Thermo-Calc model occurs at the temperature of T5 = 301°C. During crystallization, Thermo-Calc modeling shows the appearance of the ambient temperature (T7 = 50°C) of the three phases: FCC_L12, FCC_L12 # 2 and Cu_3Sn). The FCC_L12 phase is a solid solution of tin (Sn 1%) in copper (Cu 99%) which is the main component of the structure at 89.3%. The FCC_L12 # 2 phase being Pb95.6Bi4.4 phase crystallizes at T4 = 313°C and finally appears at ambient temperature in an amount of 6.8%. As a result of the interdependencies between the alloying elements, the last appearing phase at the temperature T6 = 133°C is in a small amount, amounting to 3.9%, is the CU3SN phase. The model tests carried out with the Thermo-Calc software assume the presence of LIQUID liquids in the temperature range: 1044-301°C. The experiment confirms this temperature range, however, practically the end of crystallization is at the temperature of 806°C. Due to the small amount of elements such as lead, tin or bismuth, there is some difficulty in determining the exact thermal effects based on the ATD analysis, especially in low temperature ranges.

Computer simulations

The process of reverse design, leading to the determination of the process of casting the necklace in the clay form, began with the completion of precise data about the object, constituting the necessary documentation. Laboratory data and thermophysical calculations were used for the simulation. To determine the possibilities of casting the necklace in a virtually reconstructed clay form, a simulation was performed in the MAGMASOFT® software.

The gating system was checked in several variants, so that in the final version it was adopted the version based on the necklace from the metallurgist's treasure in Uścikowiec (Fig. 15), which is the closest available analogy of the gating system for a similar type of hoop ornament with similar chronology. A two-channel gating system was used, tangent to the middle, thickest part of the necklace.

Fig. 15. The gating system with a fragment of a necklace from the treasure of a metallurgist from Uścikowiec in Wielkopolska, Bronze Age

Designing a 3D model of a necklace and casting technology

The process of recreating the casting technology began with the preparation of a 3D model of the necklace, which is shown in Fig. 16. The visualization of the necklace was made in the SOLIDWORKS CAD software.

Fig. 16. Visualization of a 3D model of the necklace in an isometric view

The prepared 3D model shown in Fig. 16 was used to prepare the casting technology. The developed casting technology on the basis of the previously prepared 3D model of the necklace is shown in Fig. 17.

The casting technology, which is shown in Fig. 17, has gates tangent to the necklace casting. A gating system designed in such a way results in a softer filling of the mould canals with liquid metal and can minimize the tearing of the mould canals due to excessive speed during the casting process.

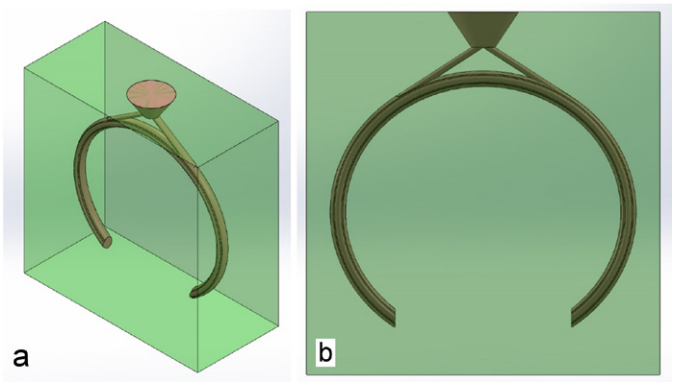

Fig. 17. Isometric view of the developed mould and casting technology in isometric view (a) and front view (b)

TABLE 5

Parameters used for the numerical simulation in the MAGMASOFT® software

The name of the parameter	Value
Casting alloy	CuSn12
Pouring temperature [°C]	1200
Mould temperature [°C]	25
Casting time [s]	1.5

Numerical simulations

The numerical simulation was performed in the MAGMASOFT® software. The individual parameters for the performed simulation are presented in TABLE 5.

Casting process

Fig. 18 shows the temperature distribution during pouring the casting mould. The results for the pour point are for a step of 42.03% (a) and 96.05% (b).

The results in Fig. 18 show that the temperature during the casting process is stable.

Fig. 19 shows the velocity distribution during pouring the canals of the casting mould. The presented results for the speed during casting process are for the step 42.03% (a) and 96.05% (b).

The velocity distribution when filling the canals of the casting mould shown in Fig. 19 does not exceed the value of 1 [m/s] and the liquid metal does not have high deviations in values when filling individual canals of the mould. The liquid metal, having the parameters shown in Fig. 19, uniformly fills the individual canals without tearing the walls of the canals of the casting mould.

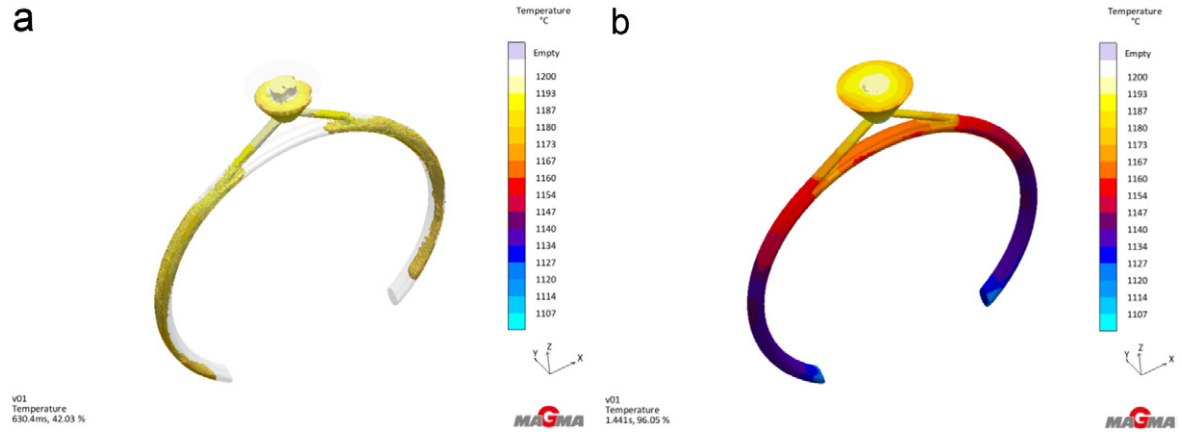

Fig. 18. Temperature distribution during the casting process: step of 42.03% (a) and 96.05% (b)

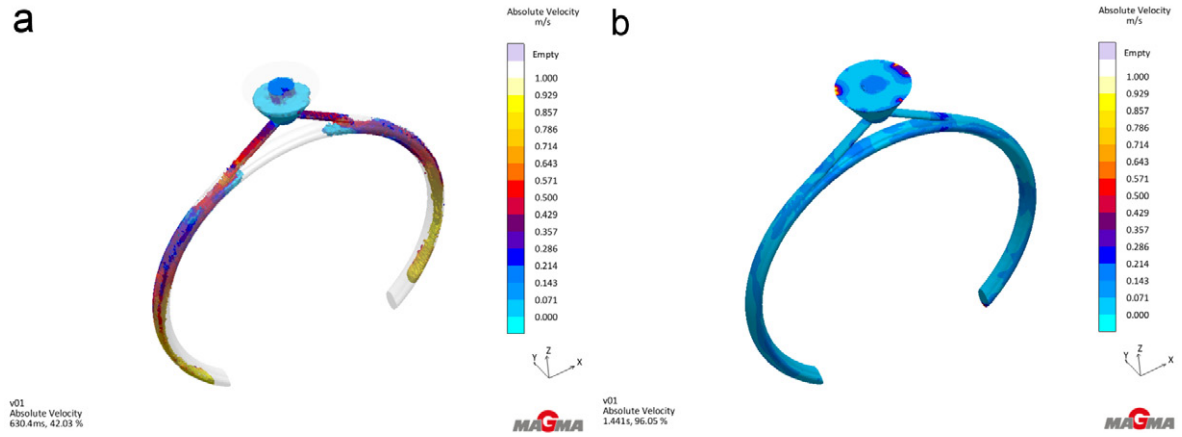

Fig. 19. Velocity distribution of liquid metal when filling the mould step: of 42.03% (a) and 96.05% (b)

Fig. 20 shows the pressure distribution during the pouring process of the casting mould. The results shown for the priming pressure are for a step of 42.03% (a) and 96.05% (b).

The pressure distribution during filling the canals of the casting mould is shown in Fig. 20 and does not exceed the value of 2000 mbar. The liquid metal does not have high values of pressure variations during pouring the mould. The liquid metal, having the pressure parameters shown in Fig. 20, uniformly fills the individual canals without damaging the walls of the mould due to high pressure fluctuations.

Solidification process

Fig. 21 shows the temperature distribution during the solidification process. The results for the temperature during the solidification process are shown for steps 42.12% (a) and 96.13% (b).

The solidification process presented in the individual steps in Fig. 6 indicates that the gates leading to the casting (a) solidify fastest having the lowest temperature values. However, with the passage of time 27.791 s (b) it can be noticed that the tempera-

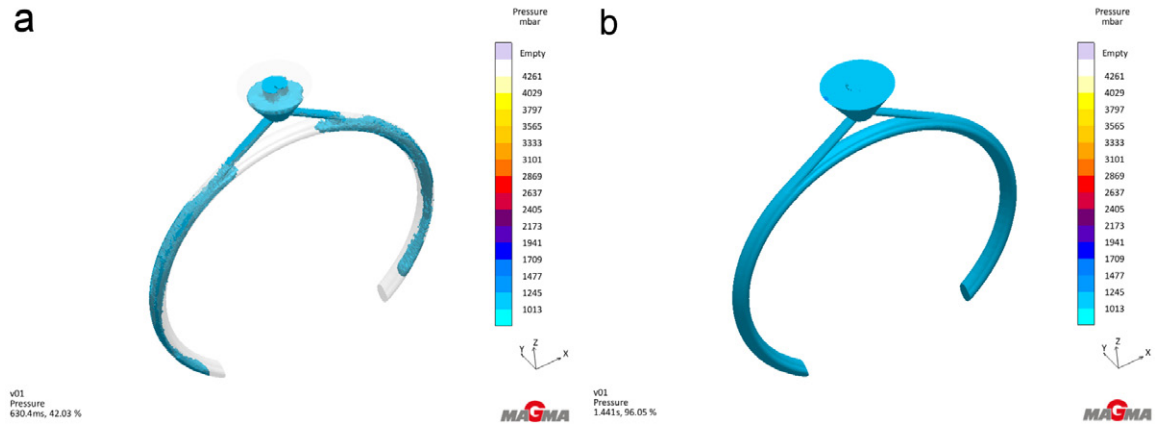

Fig. 20. Pressure distribution of liquid metal when filling the casting mould: step of 42.03% (a) and 96.05% (b)

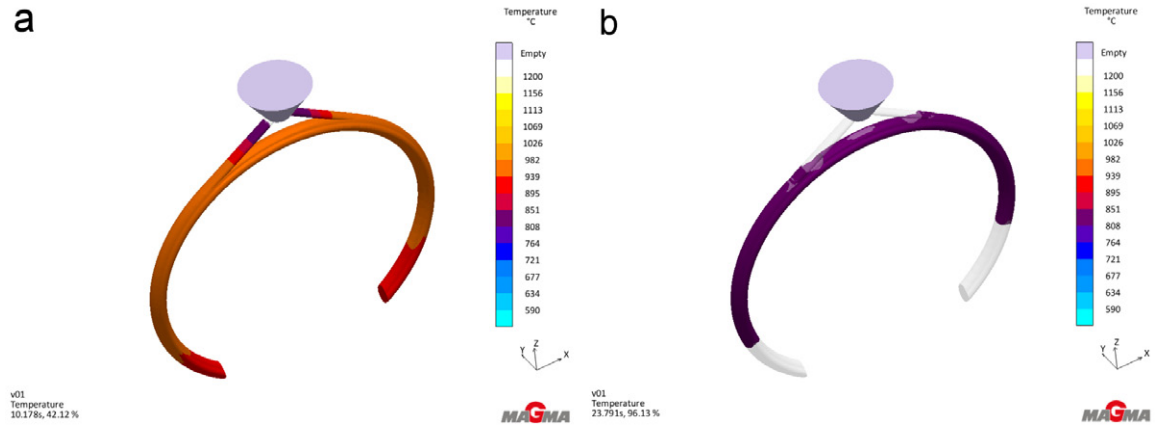

Fig. 21. Temperature distribution during the solidification process: steps 42.12% (a) and 96.13% (b)

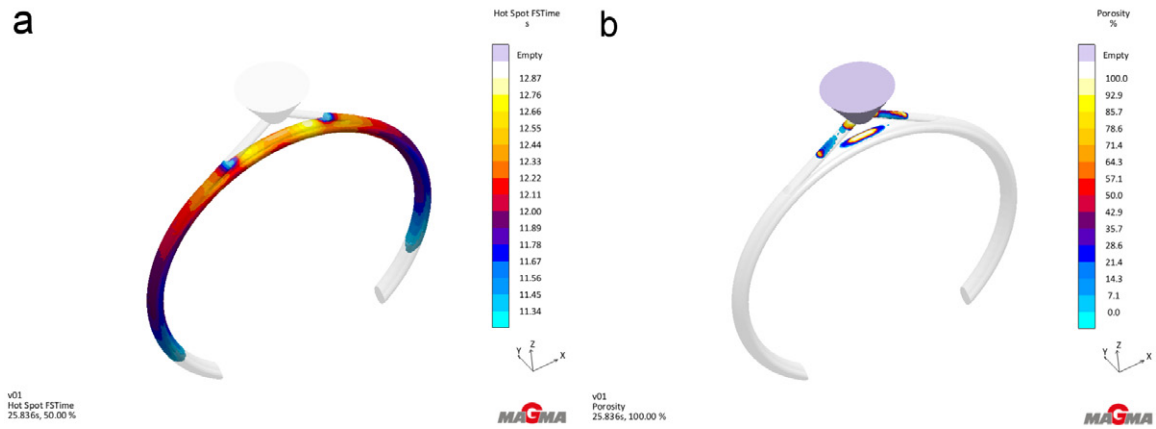

Fig. 22. Distribution of hot spots (a) and porosity (b) during the solidification process

ture does not have large deviations and amounts to about 851°C value.

Fig. 22 shows the distribution of hot spots (a) and porosity (b) during the solidification process.

Fig. 22(a) shows the hot spots formed during the solidification process. It can be seen that the highest values occur in the upper part of the casting right next to the gating system and amount to approx 12.11-12.87 s values. At these points, it can be predicted that porosity will develop.

Fig. 22(b) shows the porosity distribution. The porosity occurs in the places described in Fig. 22(a) and are the result of the hot spots formed.

The yellow circle in Fig. 23 shows the location of the defect for the real necklace casting.

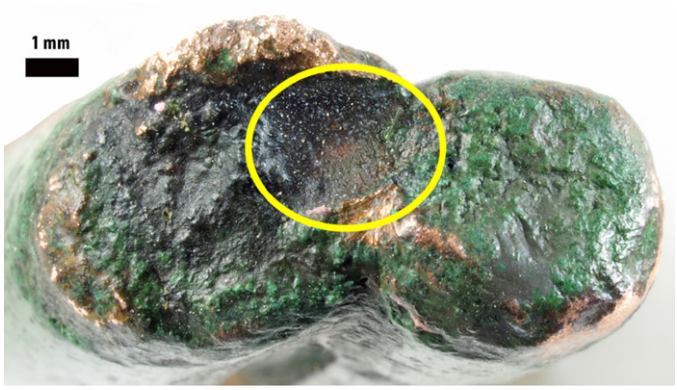

Fig. 23. Location of the defect for the actual necklace casting

The location of the resulting casting defect, which is shown in Fig. 23, presents that in this place there is a weakened cross-sectional area containing porosity. The results of the numerical simulation are very similar the place for the porosity created in the physical casting.

Fig. 22(b) shows the porosity distribution. Porosity is correlated with places which are presented in Fig. 22(a) and result from the resulting heat nodes. Fig. 23 shows a defect for an real-cast of an extensive blowhole necklace. These hole is caused due to excessive gas content in the metal bath and it takes the form of an oblong cavity caused by gases trapped by the solidifying metal in the surface layer. The blisters are usually located at the top of the casting. In Fig. 24, arrows indicate the blowhole cavity causing the necklace to break in half.

The location of the resulting casting defect, which is shown in Fig. 24, shows that there is a weakened cross-sectional area containing a bubble or significant porosity at this location. The results of the numerical simulation accurately indicate the area of the expected defect in the physical casting of the necklace.

4. Discussion

The study carried out several dozen simulations for a variable temperature of the mould: from 25 to 275, every 50°C, and a variable pouring time: from 2 to 5, every 1 second. 50 different variants of the process were analyzed. Finally, a simulation leading to the reproduction of the casting defect was selected, consistent with the actual necklace. The mould temperature was 25°C. The pouring temperature was set at 1200°C. The pouring time was set at 1.5 s. From the obtained simulation data it can be concluded that a longer pouring time causes defects in the casting in the form of visible porosity areas. With a pouring time of 2.0 s and a temperature of heating the mould before pouring to 275°C, it is possible to significantly reduce porosity and ensure a smooth (laminar) flow. However, the aim was to present the gating system design and the set casting conditions at which the defects would occur as in the real casting.

5. Conclusion

Laboratory tests and computer simulations enabled the technology to be analyzed and visualized. Analytical research, supported by theoretical and experimental thermodynamic analysis of the alloy, allowed for the collection of data that made it possible to get closer to the actual conditions of the necklace casting. The chemical profile of the necklace indicated lead bronze with a small amount of tin and additives such as bismuth, silver,

Fig. 24. Macroscopic image of the location of defect in a real artifact

arsenic and antimony. Macroscopic analysis indicates the use of the lost wax casting method in a clay form on the basis of a wax model on which geometric decorations were placed. The visible dendritic structure is also indicative of the necklace's casting process. Precipitations do not show traces of deformation as a result of plastic processing. The pictures of the necklace's microstructure show a dendritic structure with numerous precipitates of intermetallic phases. The Cu-Pb type system is characterized by the lack of mutual solubility of copper and lead components in the solid state and limited solubility in the liquid state. The solidification range of the alloy was determined theoretically and experimentally within very wide limits of 1044.4°C-301.6°C, which gives 742.8°C.

The obtained data was used in simulations of pouring and solidifying the alloy. The geometry of the casting with the gating system was obtained on the basis of the preserved fragments of the necklace and the available analogies in the form of fragments of casting moulds and gating system, which justify the adoption of the concept of pouring the necklace in the middle part by a double gating system, tangent to its circumference in the thickest part of the necklace. The tests and simulations enabled the experimental determination of the cause of the necklace damage. Undertaking this type of research on a larger scale will allow to learn the details of casting technology, such as the structure of the mould and gating system, heating the mould before pouring, pouring time and the possibility of eliminating defects in the form of porosity. In a broader sense, it will allow to develop many issues related to the production of the Bronze Age.

Funding

The financial support of the National Science Centre, Poland: 2017/26/E/HS3/00656 is acknowledged.

Conflict of Interest

The authors declare no conflicts of interest.

REFERENCES

[1] E. Pernicka, Provenance determination of metal artifacts: Methodological considerations, Nuclear Instruments and Methods in Physics Research Section B: Beam Interactions with Materials and Atoms **14** (1), 24-29 (1986).

[2] J. Lutz, E. Pernicka, E. Energy dispersive x-ray fluorescence analysis of ancient copper alloys: Empirical values for precision and accuracy, Archaeometry **38** (2), 313-323 (1996).

[3] B.S. Ottaway, Innovation, production and specialization in early prehistoric copper metallurgy, European Journal of Archaeology **4** (1), 87-112 (2001).

[4] E. Pernicka, Archaeometallurgy: Examples of the application of scientific methods to the provenance of archaeological metal objects, in: M. Martini, M. Milazzo, M. Piacentini (Eds.), Physics methods in archaeometry, Oxford: IOS Press (2004).

[5] T.L. Kienlin, Copper and Bronze Age: Bronze Age metalworking in context, in: H. Fokkens and A. Harding (Eds.),The Oxford Handbook of the European Bronze Age, Oxford, Oxford University Press (2013)

[6] V. Lyubomirova, R. Djingova, I. Kuleff, Comparison of analytical techniques for analysis of archaeological bronze, Archaeometry, 1-10 (2014).

[7] M. Radivojević, B.W. Roberts, E. Pernicka, Z. Stos-Gale, M. Martinón-Torres, T. Rehren, P. Bray, D. Brandherm, J. Ling, J. Mei, H. Vandkilde, H. Kristiansen, S.J. Shennan, C. Broodbank, The Provenance, Use, and Circulation of Metals in the European Bronze Age: The State of Debate, Journal of Archaeological Research (2018).
DOI: https://doi.org/10.1007/s10814-018-9123-9

[8] N.H. Gale, Z.A. Stos-Gale, Bronze Age Copper Sources in the Mediterranean: A New Approach, Science **216** (4541), 11-19 (1982).

[9] P. Northover, Alloy design in the Bronze Age, in: J.E. Jones (Ed.), Aspects of ancient mining and metallurgy, Bangor: University College of North Wales (1988).

[10] B.S. Ottaway, B.W. Roberts, The emergence of metallurgy, in: A. Jones (Ed.), Prehistoric Europe: Theory and practice, London: Blackwell (2008).

[11] P.J. Bray, A.M. Pollard, A new interpretative approach to the chemistry of copper-alloy objects: Source, recycling and technology, Antiquity **86** (333), 853-867 (2012).
DOI: https://doi.org/10.1017/S0003598X00047967

[12] E. Pernicka, Provenance Determination of Archaeological Metal Objects, in: Roberts B., Thornton C. (Eds.) Archaeometallurgy in Global Perspective. Springer, New York, NY (2014).
DOI: https://doi.org/10.1007/978-1-4614-9017-3_11

[13] P. Bray, A. Cuénod, C. Gosden, P. Hommel, R. Liu, A.M. Pollard, Form and flow: the 'karmic cycle' of copper, Journal of Archaeological Science **56**, 202-209 (2015).
DOI: https://doi.org/10.1016/j.jas.2014.12.013.

[14] C.J. Davey, The early history of lost-wax casting, in: J. Mei and Th. Rehren (Eds.), Metallurgy and Civilisation: Eurasia and Beyond: Proceedings of the 6th International Conference on the Beginnings of the Use of Metals and Alloys (BUMA VI), London: Archetype (2009).

[15] S. Rzadkosz, J. Zych, A. Garbacz-Klempka, M. Kranc, J. Kozana, M. Piękoś, J. Kolczyk, Ł. Jamrozowicz, T. Stolarczyk, Copper Alloys in Investment Casting Technology, Metalurgija **54** (1), 293-296 (2015).

[16] A. Garbacz-Klempka, J.S. Suchy, Z. Kwak, T. Tokarski, R. Klempka, T. Stolarczyk, Study of investment casting technology from Bronze Age : casting workshop in Grzybiany (southwest Poland), Archives of Metallurgy and Materials **63** (2), 615-624 (2018).

[17] A. Garbacz-Klempka, Ł. Kowalski, J. Kozana, J. Gackowski, M. Perek-Nowak, G. Szczepańska, M. Piękoś, Archaeometallurgical investigations of the Early Iron Age casting workshop at Kamieniec. A preliminary study, Archives of Foundry Engineering **16** (3), 29-34 (2016).

[18] E. Ciliberto, G.G. Spoto, Modern analytical methods in art and archaeology, Toronto, 2000.

[19] A. Garbacz-Klempka, Z. Kwak, P. Żak, M. Szucki, D. Ścibior, T. Stolarczyk, K. Nowak, Reconstruction of the casting technology in the Bronze Age on the basis of investigations and visualisation of casting moulds, Archives of Foundry Engineering **17** (3), 184-190 (2017).

[20] A. Garbacz-Klempka, J.S. Suchy, Z. Kwak, P. Długosz, T. Stolarczyk, Casting technology experiment and computer modeling of ornaments from Bronze Age, Archives of Metallurgy and Materials **63** (3), 1329-1337 (2018).

[21] J. Kostrzewski, Przewodnik po dziale przedhistorycznych Muzeum im. Mielżyńskich, 29 p. Poznań (1918)

[22] Inventory book of Department of Archaeology, Mielżyński Museum 1885-1920, pp.122-123, inv. No 1913:2.

[23] K. Kristansen, Europe before history. Cambridge (1998).

[24] M. Trachsel, Untersuchungen zur relativen und absoluten Chronologie der Hallstattzeit, Universitätsforschungen für prähistorische Archäologie 104, Teil 1-2, Bonn: Habelt (2004).

[25] K. Dzięgielewski, A. Garbacz-Klempka, K. Tunia, A strange specimen in an unusual place. The early iron age ring of a "Pomeranian" breastplate from smolice, oświęcim district (southern Poland), (Nietypowy okaz w nietypowym miejscu: Pierścień „pomorskiego" napierśnika z wczesne j epoki żelaza ze Smolic, pow. Oświęcim (południowa Polska)), Študijné zvesti Archeologického ústavu SAV, **1**, 127-1387 (2019).
DOI: https://doi.org/10.31577/szausav.2019.suppl.1.

[26] W. Blajer Skarby przedmiotów metalowych z epoki brązu i wczesnej epoki żelaza na ziemiach polskich. Kraków (2001).

[27] N. Saunders, A.P. Miodownik, The Cu-Sn (copper-tin) system, Bulletin of Alloy Phase Diagrams **11** (3), 278-287 (1990).
DOI: https://doi.org/10.1007/BF03029299

[28] B. Korojy, L. Ekbom, H. Fredriksson, Microsegregation and Solidification Shrinkage of Copper-Lead Base Alloys, Adv. Mater. Sci. Eng. 1-9 (2009).
DOI: https://doi.org/10.1155/2009/627937

[29] P.C. Chaubal, M. Nagamori, Thermodynamics for arsenic and antimony in copper matte converting-computer simulation, Metallurgical and Materials Transactions B **19B** (4), 547-556 (1988).
DOI: https://doi.org/10.1007/BF02659145

[30] C. Chen, L, Zhang, S. Johanshahi, Thermodynamic modeling of arsenic in copper smelting processes, Metallurgical and Materials Transactions B **41B** (6), 1175-1185 (2010).
DOI: https://doi.org/10.1007/s11663-010-9431-z

[31] E. Požega, L. Gomidželović, D. Živković, V. Trujić, The impurities behaviour analysis in thermodynamic simulation models in copper metallurgy, Journal of the University of Chemical Technology and Metallurgy **45** (2), 189-194 (2010).

[32] A. Roine, H. Jalkanen, Activities of arsenic, antimony, bismuth, and lead in copper mattes, Metallurgical and Materials Transactions B, **16B** (1), 129-41 (1985).

[33] A. Yazawa, Distribution of various elements between copper, matte, and slag, Erzmetall